Article

# Branched Coordination Multilayers on Gold

Meni Wanunu, Alexander Vaskevich, Sidney R. Cohen, Hagai Cohen, Rina Arad-Yellin, Abraham Shanzer, and Israel Rubinstein

*J. Am. Chem. Soc.*, **2005**, 127 (50), 17877-17887• DOI: 10.1021/ja0556676 • Publication Date (Web): 24 November 2005



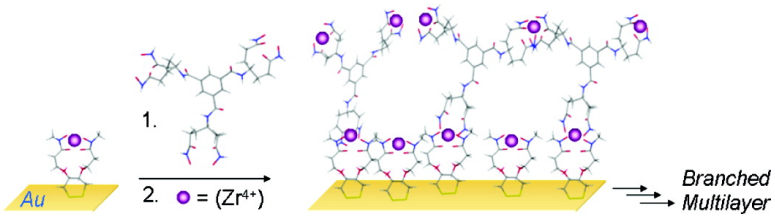


## More About This Article

Additional resources and features associated with this article are available within the HTML version:

- Supporting Information
- Links to the 13 articles that cite this article, as of the time of this article download
- Access to high resolution figures
- Links to articles and content related to this article
- Copyright permission to reproduce figures and/or text from this article

View the Full Text HTML

J|A|C|S
ARTICLES
Published on Web 11/24/2005

# Branched Coordination Multilayers on Gold

Meni Wanunu,[†] Alexander Vaskevich,[†] Sidney R. Cohen,[‡] Hagai Cohen,[‡] Rina Arad-Yellin,[§] Abraham Shanzer,[§] and Israel Rubinstein*,[†]

*Contribution from the Department of Materials and Interfaces, Department of Chemical Research Support, and Department of Organic Chemistry, Weizmann Institute of Science, Rehovot 76100, Israel*

Received August 18, 2005; E-mail: israel.rubinstein@weizmann.ac.il

***Abstract:*** A $C_3$-symmetric tridentate hexahydroxamate ligand molecule was specially synthesized and used for coordination self-assembly of branched multilayers on Au surfaces precoated with a self-assembled monolayer (SAM) of ligand anchors. Layer-by-layer (LbL) growth of multilayers via metal−organic coordination using $Zr^{4+}$ ions proceeds with high regularity, adding one molecular layer in each step, as shown by ellipsometry, wettability, UV−vis spectroscopy, and atomic force microscopy (AFM). The branched multilayer films display improved stiffness, as well as a unique defect self-repair capability, attributed to cross-linking in the layers and lateral expansion over defects during multilayer growth. Transmetalation, i.e., exposure of $Zr^{4+}$-based assemblies to $Hf^{4+}$ ions, was used to evaluate the cross-linking. Conductive atomic force microscopy (AFM) was used to probe the electrical properties of the multilayers, revealing excellent dielectric behavior. The special properties of the branched layers were emphasized by comparison with analogous multilayers prepared similarly using linear (tetrahydroxamate) ligand molecules. The process of defect annihilation by bridging over defective areas, attributed to lateral expansion via the excess bishydroxamate groups, was demonstrated by introduction of artificial defects in the anchor monolayer, followed by assembly of two layers of either the linear or the branched molecule. Analysis of selective binding of Au nanoparticles (NPs) to unblocked defects emphasized the superior repair mechanism in the branched layers with respect to the linear ones.

## Introduction

Layer-by-layer (LbL) construction of multilayer films on surfaces offers several advantages with respect to other deposition schemes, providing superior control over film thickness and composition in the vertical direction, which determine the multilayer properties. Several systems of this kind have been developed, distinguished by the type of interaction between the layers. The Langmuir−Blodgett technique for the generation of multilayers is the earliest reported form of molecularly controlled deposition.[1] Covalent assembly from solution was presented by Sagiv and coworkers, who utilized bifunctional organosilanes to prepare multilayers in a LbL fashion.[2] Other types of covalent multilayer assembly schemes were developed later.[3−8] Electrostatic self-assembly, a commonly used technique for the generation of thin films, was first realized by Iler[9] and later adopted to polymers by Decher and co-workers.[10,11] Hydrogen-bonding interactions have also shown utility in the construction of multilayers.[12−14] LbL multilayer formation by metal ion coordination using bifunctional ligand building blocks has been studied in a variety of systems, including mercaptocarboxylate/Cu(II),[15] diphosphonate/M(IV),[16−23] amine/Pt(II),[24] Co(II)/diisocyanide,[25] $Ru_3$-cluster/bipyridyl,[26] tetrahydroxamate/

[†] Department of Materials and Interfaces.
[‡] Department of Chemical Research Support.
[§] Department of Organic Chemistry.

(1) Blodgett, K. B. *J. Am. Chem. Soc.* **1934**, *56*, 495−495.
(2) Netzer, L.; Sagiv, J. *J. Am. Chem. Soc.* **1983**, *105*, 674−676.
(3) Kohli, P.; Taylor, K. K.; Harris, J. J.; Blanchard, G. J. *J. Am. Chem. Soc.* **1998**, *120*, 11962−11968.
(4) Wang, Y.; Wang, X. J.; Guo, Y.; Cui, Z. C.; Lin, Q.; Yu, W. Z.; Liu, L. Y.; Xu, L.; Zhang, D. M.; Yang, B. *Langmuir* **2004**, *20*, 8952−8954.
(5) Zhang, S. X.; Yang, W. W.; Niu, Y. M.; Sun, C. Q. *Anal. Chim. Acta* **2004**, *523*, 209−217.
(6) Liang, Z. Q.; Wang, Q. *Langmuir* **2004**, *20*, 9600−9606.
(7) Bocking, T.; James, M.; Coster, H. G. L.; Chilcott, T. C.; Barrow, K. D. *Langmuir* **2004**, *20*, 9227−9235.
(8) Zhang, J. S.; Xu, L.; Cui, Y.; Cao, W. X.; Li, Z. *Mater. Chem. Phys.* **2005**, *90*, 47−52.
(9) Iler, R. K. *J. Colloid Interface Sci.* **1966**, *21*, 569−594.
(10) Decher, G.; Hong, J. D. *Makromol. Chem. Macromol. Symp.* **1991**, *46*, 321−327.
(11) Decher, G.; Schlenoff, J. B. *Multilayer Thin Films: Sequential Assembly of Nanocomposite Materials*; Wiley-VCH: Weinheim, Germany, 2003.
(12) Stockton, W. B.; Rubner, M. F. *Macromolecules* **1997**, *30*, 2717−2725.
(13) Wang, L. Y.; Wang, Z. Q.; Zhang, X.; Shen, J. C.; Chi, L. F.; Fuchs, H. *Macromol. Rapid Commun.* **1997**, *18*, 509−514.
(14) Zhang, H. Y.; Wang, Z. Q.; Zhang, Y. Q.; Zhang, X. *Langmuir* **2004**, *20*, 9366−9370.
(15) Evans, S. D.; Ulman, A.; Goppertberarducci, K. E.; Gerenser, L. J. *J. Am. Chem. Soc.* **1991**, *113*, 5866−5868.
(16) Lee, H.; Kepley, L. J.; Hong, H. G.; Mallouk, T. E. *J. Am. Chem. Soc.* **1988**, *110*, 618−620.
(17) Katz, H. E.; Scheller, G.; Putvinski, T. M.; Schilling, M. L.; Wilson, W. L.; Chidsey, C. E. D. *Science* **1991**, *254*, 1485−1487.
(18) Kepley, L. J.; Sackett, D. D.; Bell, C. M.; Mallouk, T. E. *Thin Solid Films* **1992**, *208*, 132−136.
(19) Umemura, Y.; Tanaka, K.; Yamagishi, A. *J. Chem. Soc.* **1992**, 67−68.
(20) Katz, H. E.; Schilling, M. L. *Chem. Mater.* **1993**, *5*, 1162−1166.
(21) Zeppenfeld, A. C.; Fiddler, S. L.; Ham, W. K.; Klopfenstein, B. J.; Page, C. J. *J. Am. Chem. Soc.* **1994**, *116*, 9158−9165.
(22) Hanken, H. G.; Corn, R. M. *Anal. Chem.* **1995**, *67*, 3767−3774.
(23) Hatzor, A.; van der Boom-Moav, T.; Yochelis, S.; Vaskevich, A.; Shanzer, A.; Rubinstein, I. *Langmuir* **2000**, *16*, 4420−4423.
(24) Watanabe, S.; Regen, S. L. *J. Am. Chem. Soc.* **1994**, *116*, 8855−8856.
(25) Ansell, M. A.; Cogan, E. B.; Neff, G. A.; von Roeschlaub, R.; Page, C. J. *Supramol. Sci.* **1997**, *4*, 21−26.

M(IV),[27−29] and other systems.[30,31] Metal ion coordination was also demonstrated in ligand-containing polyelectrolyte multilayer films.[32] The importance of precise control over film thickness and composition was recently highlighted by the fabrication of several-nanometer-thick multilayers used as dielectrics for organic thin film transistors.[33]

The various strategies for multilayer construction present advantages as well as disadvantages. For example, LbL deposition of polyelectrolyte films is widely used, benefiting from the abundance of charged polymers and other building blocks.[34] However, such assemblies are known to present an irregular morphology, resulting in interdigitation of the layers and typically an increased film permeability with increasing number of layers.[35] On the other hand, multilayers composed of bifunctional molecules are presumed to grow in a lamellar mode. Such schemes were utilized, e.g., in the construction of asymmetric multilayers, displaying nonlinear optical properties.[36] However, unavoidable pinholes, adsorbed impurities, surface roughness, grain boundaries, and inherent tilt of various molecules, lead to deleterious accumulation of defects with added layers, limiting the applicability of LbL multilayers.[37,38] For example, electronic applications of multilayer films require pinhole-free layers to avoid short-circuits between top and bottom contacts.[39,40]

A possible approach to overcoming the defect accumulation problem is introduction of branching in the layers, thus providing a self-healing mechanism and the possibility of bridging over defects. This, however, may lead to an irregular film structure, as branching is likely to promote uncontrolled growth. Several approaches have been demonstrated to the preparation of hyperbranched polymer films on surfaces for sensing, control over functional group density, and corrosion protection.[41−45] A recent report on film construction by nonlinearly directed supramolecular recognition showed ordered multilayer growth, but rather low film homogeneity, as seen by atomic force microscopy (AFM).[46]

In the present work, branched multilayers exhibiting molecular-scale control over film thickness and a high degree of homogeneity are presented. The distinct features deriving from this construction are expressed in the structural and mechanical properties of the films. The branched films are based on a custom-synthesized $C_3$-symmetrical hexahydroxamate tridentate molecule consisting of three bis-hydroxamate ion-binding sites. We show that the branched building block can yield a regular multilayer growth mode, similar to that of analogous linear (tetrahydroxamate) building blocks, the latter providing two bis-hydroxamate binding sites. LbL multilayers were prepared by coordination self-assembly on Au substrates using $Zr^{4+}$ ions, and their morphology, mechanical, and electrical properties have been investigated and compared to those of the analogous linear multilayers.

A unique feature of the branching is possible lateral expansion via the excess functional groups, thus providing an effective defect self-repair mechanism during multilayer growth. To demonstrate this effect a mixed self-assembled monolayer (SAM) comprising the anchor ligand and alkanedithiol molecules, the latter serving as simulated defects, was constructed. Further assembly of either branched or linear coordination building blocks, followed by binding of Au nanoparticles (NPs) to remaining dithiol defects, revealed an efficient defect elimination mechanism in the branched multilayer.

## Experimental Section

**Chemicals and Materials.** All solvents and reagents were analytical grade and used as received. Chloroform (AR, Biolab) was passed through a column of activated basic alumina prior to use. Octadecylmercaptan (OM) (98%, Aldrich) was recrystallized from ethanol prior to use. Water was triply distilled. Samples were dried using 0.2 $\mu$m PTFE-filtered household $N_2$ (>99%, from liquid $N_2$).

**Au Substrates.** Transmission surface plasmon resonance (T-SPR) kinetic measurements[47] were performed on 5.0 nm Au island films prepared by evaporation (at 0.005 nm/sec) on silanized glass and annealed at 200 °C for 20 h.[48] The substrates in all other experiments were semitransparent, continuous Au films (~17 nm thick), prepared by evaporation (at 0.05 nm/sec) on aminosilane-treated glass or quartz and annealed at 200 °C for 20 h.[49]

**Adsorption Conditions.** Figure 1a shows the building blocks **1**−**3** used in this work. Figure 1b shows the construction scheme used for coordination self-assembly of multilayers of **1**. SAMs of **2** were prepared by overnight adsorption in a 3 mM solution of **2** in 1:1 EtOH/$CHCl_3$.[50] Binding of $Zr^{4+}$ or $Hf^{4+}$ was carried out by 1 h immersion in a fresh 1 mM ethanolic solution of $Zr(acac)_4$ or $Hf(acac)_4$, respectively, followed by rinsing in EtOH and drying under $N_2$.[29] Transmetalation experiments were performed according to the sequences in Table 2, with rinsing and drying following each adsorption step. Binding of **1** was accomplished by overnight immersion in a 3 mM methanolic solution of **1**, followed by rinsing in MeOH and drying under $N_2$. Binding of **3** was performed by overnight immersion in a 3 mM ethanolic solution of **3**, followed by rinsing in EtOH and drying under $N_2$.[29] Binding of $Cu^{2+}$ ions for blank experiments was accomplished by 1 h immersion in a 1 mM ethanolic solution of $Cu(ClO_4)_2$.


(26) Abe, M.; Michi, T.; Sato, A.; Kondo, T.; Zhou, W.; Ye, S.; Uosaki, K.; Sasaki, Y. *Angew. Chem., Int. Ed.* **2003**, *42*, 2912−2915.
(27) Hatzor, A.; Moav, T.; Cohen, H.; Matlis, S.; Libman, J.; Vaskevich, A.; Shanzer, A.; Rubinstein, I. *J. Am. Chem. Soc.* **1998**, *120*, 13469−13477.
(28) Doron-Mor, H.; Hatzor, A.; Vaskevich, A.; van der Boom-Moav, T.; Shanzer, A.; Rubinstein, I.; Cohen, H. *Nature* **2000**, *406*, 382−385.
(29) Doron-Mor, I.; Cohen, H.; Cohen, S. R.; Popovitz-Biro, R.; Shanzer, A.; Vaskevich, A.; Rubinstein, I. *Langmuir* **2004**, *20*, 10727−10733.
(30) Byrd, H.; Holloway, C. E.; Pogue, J.; Kircus, S.; Advincula, R. C.; Knoll, W. *Langmuir* **2000**, *16*, 10322−10328.
(31) Thomsen, D. L.; Phely-Bobin, T.; Papadimitrakopoulos, F. *J. Am. Chem. Soc.* **1998**, *120*, 6177−6178.
(32) Krass, H.; Papastavrou, G.; Kurth, D. G. *Chem. Mater.* **2003**, *15*, 196−203.
(33) Yoon, M. H.; Facchetti, A.; Marks, T. J. *Proc. Natl. Acad. Sci. U.S.A.* **2005**, *102*, 4678−4682.
(34) Hammond, P. T. *Adv. Mater.* **2004**, *16*, 1271−1293.
(35) Von Klitzing, R.; Wong, J. E.; Jaeger, W.; Steitz, R. *Curr. Opin. Colloid Interface Sci.* **2004**, *9*, 158−162.
(36) Li, D. Q.; Ratner, M. A.; Marks, T. J.; Zhang, C. H.; Yang, J.; Wong, G. K. *J. Am. Chem. Soc.* **1990**, *112*, 7389−7390.
(37) Pomerantz, M.; Segmuller, A.; Netzer, L.; Sagiv, J. *Thin Solid Films* **1985**, *132*, 153−162.
(38) Tredgold, R. H. *Order in Thin Organic Films*; Cambridge University Press: Cambridge, 1994.
(39) Polymeropoulos, E. E.; Sagiv, J. *J. Chem. Phys.* **1978**, *69*, 1836−1847.
(40) Baker, M. V.; Landau, J. *Aust. J. Chem.* **1995**, *48*, 1201−1211.
(41) Zhou, Y. F.; Bruening, M. L.; Bergbreiter, D. E.; Crooks, R. M.; Wells, M. *J. Am. Chem. Soc.* **1996**, *118*, 3773−3774.
(42) Bruening, M. L.; Zhou, Y. F.; Aguilar, G.; Agee, R.; Bergbreiter, D. E.; Crooks, R. M. *Langmuir* **1997**, *13*, 770−778.
(43) Zhang, L.; Bo, Z. S.; Zhao, B.; Wu, Y. Q.; Zhang, X.; Shen, J. C. *Thin Solid Films* **1998**, *329*, 221−223.
(44) Kim, H. J.; Moon, J. H.; Park, J. W. *J. Colloid Interface Sci.* **2000**, *227*, 247−249.
(45) Beyerlein, D.; Belge, G.; Eichhorn, K. J.; Gauglitz, G.; Grundke, K.; Voit, B. *Macromol. Symp.* **2001**, *164*, 117−131.
(46) Crespo-Biel, O.; Dordi, B.; Reinhoudt, D. N.; Huskens, J. *J. Am. Chem. Soc.* **2005**, *127*, 7594−7600.
(47) Kalyuzhny, G.; Vaskevich, A.; Schneeweiss, M. A.; Rubinstein, I. *Chem. Eur. J.* **2002**, *8*, 3850−3857.
(48) Doron-Mor, I.; Barkay, Z.; Filip-Granit, N.; Vaskevich, A.; Rubinstein, I. *Chem. Mater.* **2004**, *16*, 3476−3483.
(49) Wanunu, M.; Vaskevich, A.; Rubinstein, I. *J. Am. Chem. Soc.* **2004**, *126*, 5569−5576.
(50) Moav, T.; Hatzor, A.; Cohen, H.; Libman, J.; Rubinstein, I.; Shanzer, A. *Chem. Eur. J.* **1998**, *4*, 502−507.

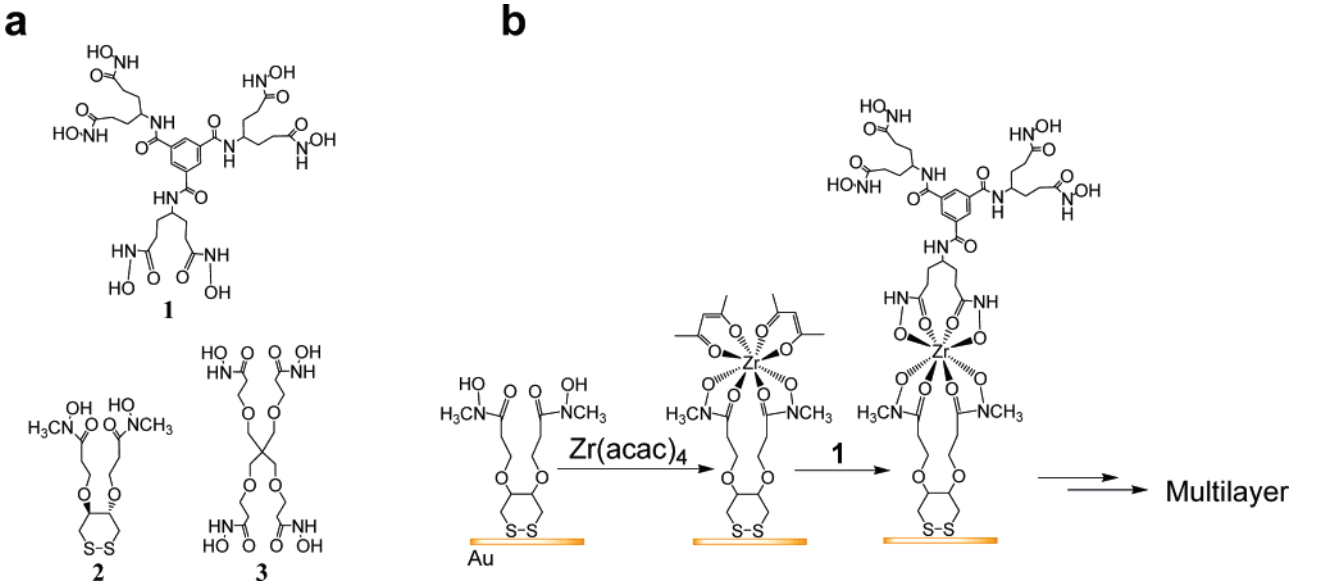


***Figure 1.*** (a) Chemical structures of molecules **1**, **2**, and **3**. (b) Schematic presentation of the stepwise construction of a $Zr^{4+}$-coordinated multilayer of **1** on a SAM of **2**. Only one of several possible binding modes of **1** is shown (see text).

**Ellipsometry.** Ellipsometric measurements were carried out with a Rudolph Research Auto-EL IV null ellipsometer, at an angle of incidence $\phi = 70°$ and a wavelength $\lambda = 632.8$ nm. The same four points were measured on each sample before and after self-assembly.

**Contact Angle (CA) Measurements.** Advancing water CAs were measured using a computerized CA meter (KSV Instruments, Finland). Data collection and analysis were carried out using the manufacturer's CAM100 software. CAs were measured on three different spots in each sample.

**Transmission UV−Vis Spectroscopy.** Transmission spectra were obtained with a Varian Cary 50 UV−vis spectrophotometer. T-SPR adsorption kinetics[47] were measured by placing the Au island substrate in a quartz cell filled with methanol, followed by injection of a concentrated methanolic solution of **1** to make a final concentration of 3 mM. A similar experiment was performed for $Zr^{4+}$ binding by injecting a concentrated solution of $Zr(acac)_4$ in ethanol, to make a final concentration of 1 mM. All other measurements were carried out in air, using a homemade holder designed for reproducibility of the sampled spot. Spectra were recorded using air as baseline.

**Atomic Force Microscopy (AFM).** Appropriate Si cantilever probes (Mikromasch, Estonia) were selected for each type of experiment. Dynamic mode AFM imaging of multilayers was performed using a PicoSPM instrument (Molecular Imaging, U.S.A.), using NSC12 cantilever probes with a resonant frequency of ca. 120 kHz. The effect of normal load on shear and wear of the multilayers was measured with a Solver P47 AFM (NT-MDT, Zelenograd, Russia). A CSC12 (tip A) probe was used with normal force constant of 1.5 N/m, as evaluated using the unloaded resonance technique,[51] with cantilever length and width evaluated from SEM micrographs. For these measurements, a 2.5 $\mu m^2$ region was first imaged in the dynamic mode at 1 Hz, then a 700 $nm^2$ window in the middle of the larger area was scanned at 2 Hz in the contact mode, while recording both lateral and total normal force. Following each scan in the contact mode, the larger area was again scanned in the dynamic mode. The procedure was repeated at increasing normal forces until the film was worn away, as evidenced by exposure of the underlying Au substrate over a significant part of the scanned region. The normal film wear force was determined as the force required to completely wear the film. Relative frictional forces were determined by comparing the lateral deflection signal levels in right-going and left-going friction traces in the acquired images. Measurements were made using a single probe and unchanged laser alignment, to ensure a valid comparison between the different films. The results for the multilayer films were compared with those for a SAM of OM on a similar Au substrate. Film thickness was determined by AFM imaging of the depth of the worn areas, prepared as described above. The reported AFM film thicknesses were calculated by averaging 10−15 line scans through the worn film. Conductive AFM measurements were carried out at 296 ± 1K and 40 ± 10% relative humidity, using a Pt-coated Si tip (NSC14/Pt) at a feedback contact force of ~2 nN. The tip was grounded and the sample bias was controlled using the STM circuitry of the PicoSPM. *I*−*V* curves were obtained on 20 points in different regions of each sample. The same tip was used for all multilayer samples.

**X-ray Photoelectron Spectroscopy (XPS).** XPS measurements were carried out with a Kratos AXIS-HS system, using monochromatized Al (Kα) X-ray source ($h\nu = 1486.6$ eV). To minimize beam-induced damage, a low dose was maintained, using a relatively low beam flux (5 mA emission current at 15 keV) and medium energy resolution (pass energy of 80 eV). The attenuated Au signal was used to calculate the thickness of the multilayer films, using an electron mean free path $\lambda = 3.3$ nm, a value typically reported for thin organic films.[52]

**Au Nanoparticle (NP) Blocking Experiments.** Mixed SAMs of **2** and 1,10-decanedithiol (DDT) were prepared by 1 h immersion of a SAM of **2** into a 1 mM ethanolic DDT solution. Subsequent coordination binding of two layers of either **1** or **3** was then carried out under conditions as detailed above. Au NPs (5 nm average core diameter) stabilized with tetraoctylammonium bromide (TOAB) were prepared using the procedure of Brust et al., i.e., biphasic reduction of $HAuCl_4$.[53] The resulting NPs were bound to the different types of films by overnight immersion in a ~1 mg/mL solution of the NPs in toluene, followed by copious rinsing, 30 s of sonication, and a 20 min of immersion in stirred toluene.

## Results and Discussion

**Synthesis of 1.** The synthesis of the $C_3$-symmetric tridentate hexahydroxamate ligand **1** (Figure 1a) is outlined in Figure 2a, and the detailed synthesis is described in the Supporting Information. Starting from 4-ketopimelic acid, the reaction

(51) Sader, J. E.; Chon, J. W. M.; Mulvaney, P. *Rev. Sci. Instrum.* **1999**, *70*, 3967−3969.

(52) Briggs, D., Seah, M. P., Eds. *Practical Surface Analysis*, 2nd ed.; Wiley: New York, 1990; Vol. 1.

(53) Brust, M.; Bethell, D.; Schiffrin, D. J.; Kiely, C. J. *Adv. Mater.* **1995**, *7*, 795−797.

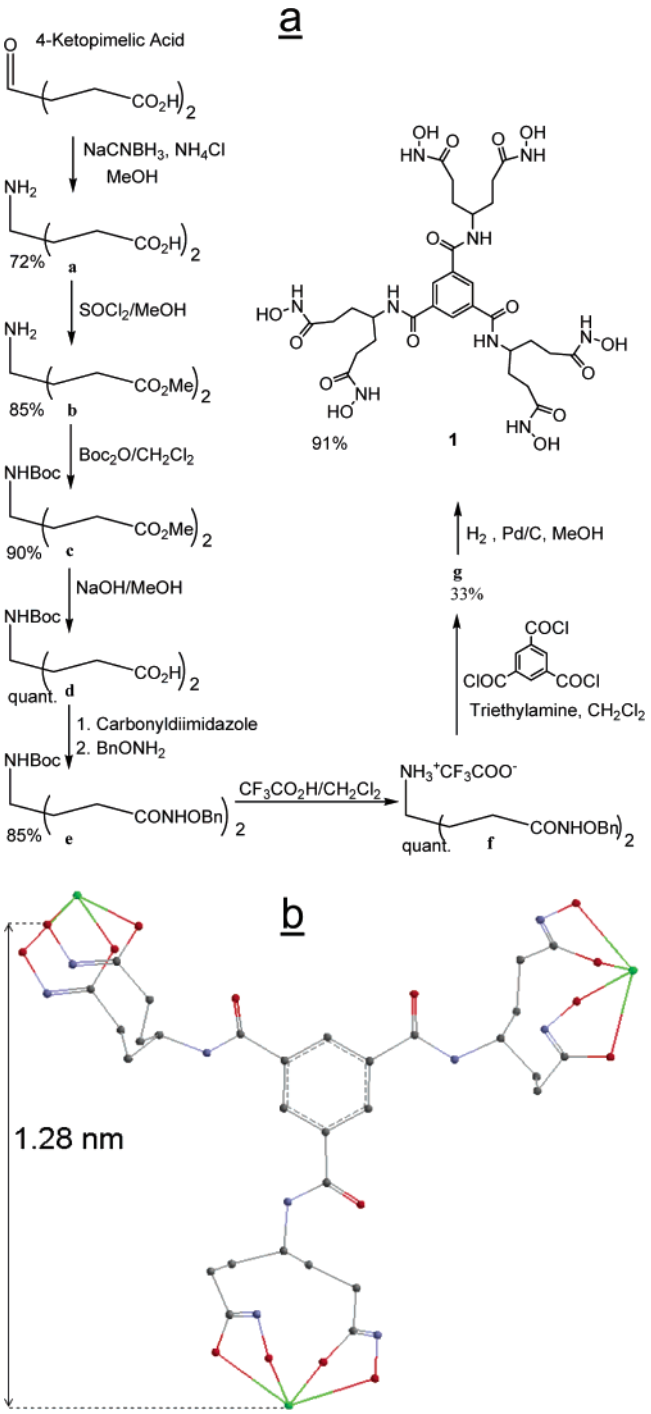


***Figure 2.*** (a) Synthetic route to the preparation of **1**. (b) Molecular model of the **1**/$Zr^{4+}$ 1:3 complex.

proceeded in eight steps with an overall yield of 15%. The structure of **1** was confirmed by FAB/HRMS, ES/MS, $^1$H NMR, and FTIR (see the Supporting Information). The chelating ability of **1** was tested by precipitation from methanol upon addition of $Cu(ClO_4)_2$ (blue precipitate), $FeCl_3$ (red precipitate), or $ZrCl_4$ (white precipitate), yielding insoluble complexes and oligomeric products.

An energy-minimized model of **1** coordinated to a $Zr^{4+}$ ion at each bis-hydroxamate binding site is shown in Figure 2b.[54] The projection height for $Zr^{4+}$-coordinated **1** is 1.28 nm, which

(54) The model was drawn using PC Spartan Pro, Wavefunction, Inc.

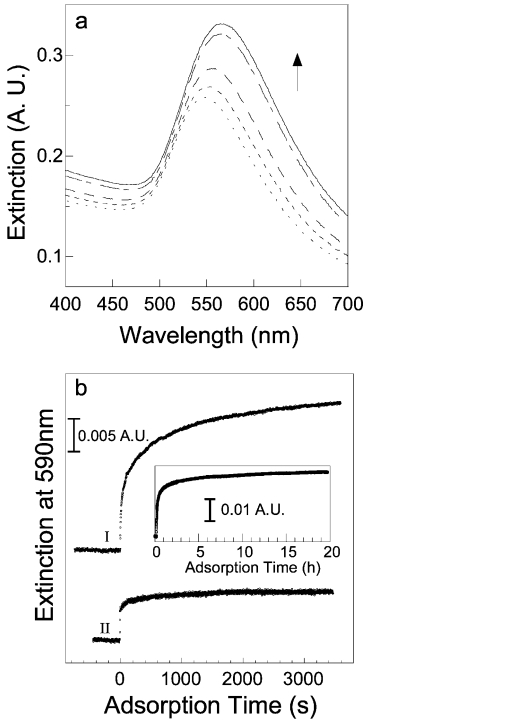


***Figure 3.*** (a)Transmission UV−vis spectra (in air) of a Au island film following the initial steps in multilayer assembly in the following order: bare Au (bottom curve), a SAM of **2**, binding of $Zr(acac)_4$, **1**, and $Zr(acac)_4$ (top curve). (b) In situ T-SPR adsorption kinetics (change in the extinction at 590 nm) of **1** (I) and subsequent adsorption of $Zr(acac)_4$ (II) onto an ultrathin Au island film derivatized with a $Zr^{4+}$-coordinated SAM of **2**. Inset: Overnight adsorption kinetics of **1**, as in I.

is the expected thickness increment per layer in a coordinated multilayer of **1** assuming a perpendicular orientation of the ligands.

**Branched Coordination Multilayers.** The construction of coordination multilayers of **1** on Au is outlined schematically in Figure 1b. The first step is functionalization of the surface with hydroxamate groups, accomplished by preparing a SAM of **2** (the anchor layer) on Au, as described previously.[50] Introduction of tetravalent metal ions (e.g., $Zr^{4+}$) followed by binding of ligand **1** provides the first branched layer. A branched coordination multilayer is achieved by subsequent alternate binding of the metal ions and ligand **1**,[55] as shown previously for analogous linear (nonbranched) coordination multilayers.[27−29] The branched multilayers grow in a highly regular manner, as shown below. Substitution of acetylacetonate (acac) groups with hydroxamates has been observed previously both on Au surface[29] and in solution.[50]

The initial steps in multilayer growth were followed by T-SPR spectroscopy using an ultrathin Au island film on glass as the substrate.[47] Figure 3a presents transmission UV−vis spectra taken after each step, starting with the bare Au and ending with one $Zr^{4+}$-coordinated layer of **1**. The spectra show increase of the Au surface plasmon (SP) band intensity in each binding step, indicating successful film deposition. The T-SPR results are in agreement with previous data on a similar system.[56]

(55) To verify that multilayer growth requires a tetravalent ion ($Zr^{4+}$, $Hf^{4+}$), $Cu^{2+}$ ions were bound to a SAM of **2**, followed by sequential immersion into **1** and $Cu^{2+}$ solution. No growth was observed following three such immersion sequences, as monitored by ellipsometry.

(56) Doron-Mor, I.; Cohen, H.; Barkay, Z.; Shanzer, A.; Vaskevich, A.; Rubinstein, I. *Chem. Eur. J.* **2005**, *11*, 5555−5562.

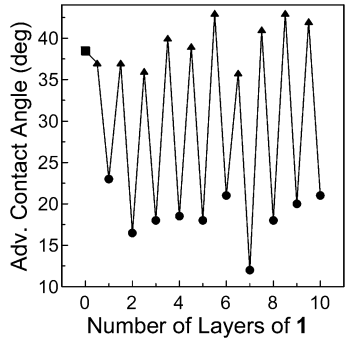


***Figure 4.*** Advancing water contact angles during multilayer construction: a SAM of **2** (square) followed by alternate exposure to $Zr(acac)_4$ (triangles) and **1** (circles).

Formation of a well-organized LbL multilayer requires optimization of the adsorption conditions, to ensure binding of a single, complete layer in each step. Therefore, the binding kinetics of **1** onto a $Zr^{4+}$-terminated surface and of $Zr^{4+}$ onto a **1**-terminated surface were investigated by in situ monitoring of the change in the SP band intensity measured at a single wavelength (Figure 3b).[47,57] Upon injection of a solution of **1** into the cell (curve I), a sharp rise in the Au SP intensity is observed, followed by a slower, steady rise which stabilizes after 17−20 h (Figure 3b, inset), indicating that overnight immersion is necessary for obtaining a complete monolayer of **1**. The binding kinetics of $Zr^{4+}$ ions to the hydroxamate-terminated layer of **1** are shown in curve II of Figure 3b. Complete binding of $Zr^{4+}$ to **1** is achieved much faster than complete binding of **1**, as indicated by the relatively fast stabilization of the SP extinction intensity. This, together with XPS results (see below), indicates that 1 h adsorption is sufficient for complete coordination of $Zr^{4+}$ to the surface.

There is a large difference (more than an order-of-magnitude) in the time required for formation of complete layers of **1** and of $Zr^{4+}$, even though the chemistry is the same (bishydroxamate−$Zr^{4+}$ coordination upon removal of two acac ligands) and mass-transport effects are negligible for a monolayer coverage. The results therefore suggest two-step adsorption kinetics for the formation of a monolayer of **1**: the majority of molecules in the layer (60−70%) are bound in the first several minutes, followed by slow insertion of the remaining molecules, eventually forming a compact monolayer in several hours. This mode has been observed with other monolayer systems, rationalized by the ability of the molecules in the layer to rearrange, exposing further surface binding sites.[58−61] The difference in the observed adsorption kinetics of **1** and $Zr^{4+}$ may therefore be explained by the slower rearrangement of **1** compared to that of $Zr(acac)_4$.

Advancing water CA data for the multilayer construction are shown in Figure 4. The CAs are sensitive to the different binding steps, showing an oscillatory behavior[27,29] between $18 \pm 4°$ and $36 \pm 3°$ for hydroxamate-terminated and $Zr^{4+}$-terminated surfaces, respectively, indicating regular multilayer growth. The decreased hydrophilicity following $Zr^{4+}$ binding is explained by replacement of surface hydroxamate groups with the more hydrophobic acac ligand (see Figure 1b). No significant decrease in the contact angles is observed with increasing number of layers, suggesting that the surface roughness is preserved.[62]

***Table 1.*** XPS Atomic Concentration Percent at Different Takeoff Angles for a 5-Layer and 10-Layer $Zr^{4+}$-Coordinated Multilayer of **1** Assembled on a SAM of **2** on Au

| system | takeoff angle (deg) | C | O | N | Zr | S | Au |
|---|---|---|---|---|---|---|---|
| Au/**2**/($Zr^{4+}$/**1**)$_5$ | 90 | 51.5 | 25.8 | 11.8 | 3.1 | 0.9 | 6.3 |
| Au/**2**/($Zr^{4+}$/**1**)$_5$ | 35 | 54.3 | 26.8 | 11.4 | 3.3 | 0.4 | 3.4 |
| Au/**2**/($Zr^{4+}$/**1**)$_{10}$ | 90 | 56.6 | 26.7 | 11.3 | 2.9 | 0.9 | 1.4 |
| Au/**2**/($Zr^{4+}$/**1**)$_{10}$ | 35 | 57.5 | 27.9 | 11.2 | 2.8 | 0.4 | 0.4 |

Multilayer growth was monitored by XPS during LbL assembly of $Zr^{4+}$-coordinated multilayers of **1** on a SAM of **2** on Au. Table 1 shows XPS atomic concentrations for 5-layer and 10-layer $Zr^{4+}$-coordinated multilayers. The results indicate formation of a uniform overlayer structure, deduced from the lack of angle dependence for the overlayer atoms (i.e., excluding S and Au) for both the 5-layer and 10-layer multilayers. The observed N/Zr ratio in the different measurements was 3.5−4.0. In a saturated, noncross-linked multilayer of **1**/$Zr^{4+}$ the repeat unit is a molecule of **1** bound to two $Zr^{4+}$ ions, i.e., one $Zr^{4+}$ connecting to the previous layer and the other bound to a free arm, leaving the third arm available for binding the next layer. This gives an N/Zr ratio of 4.5, i.e., 12−28% higher than the observed value. This difference cannot be attributed to cross-linking, which would increase the ratio due to sharing of $Zr^{4+}$ ions between neighboring molecules and is therefore assumed to indicate some residual $Zr^{4+}$ accumulated in the multilayer.[29] Overall, the XPS results confirm the formation of a spatially homogeneous multilayer structure.

The morphology of multilayer films of **1** was investigated by dynamic mode AFM, as shown in Figure 5. The semitransparent Au substrates are {111}-textured and consist of 200−500 nm wide Au single-crystal grains, as previously described.[49] Figure 5a shows a $3 \times 3\ \mu m^2$ AFM image obtained after removal of a square window from the multilayer film using the AFM tip (see the Experimental Section). The image shows that the film morphology is superimposed on the grain structure of the Au substrate. Cross sections such as the one shown in Figure 5b, performed on films with varying number of layers, show a uniform thickness increment of 1.3 nm per layer, in good agreement with film thickness measurements using other techniques (see below). A higher resolution image (Figure 5c) shows that the multilayer film is rather smooth, the concavities arising from grain boundaries of the Au substrate (see arrows). RMS roughness analysis was performed on individual Au grains, showing a relatively constant roughness value of 0.5−0.6 nm (Figure 5d), not significantly higher than the roughness of the bare Au. This is in agreement with the contact angle results (Figure 4) discussed above.

The regularity of multilayer growth was monitored optically by transmission UV−vis spectroscopy and ellipsometry. Molecule **1** absorbs light in the far UV region (see inset of Figure 6a) showing a peak at 208 nm with a molar extinction coefficient $\epsilon_{208} = 2.9 \times 10^4\ M^{-1}\ cm^{-1}$, measured in aqueous solution. The high $\epsilon$ value enabled monitoring the LbL assembly of a

(57) Kalyuzhny, G.; Schneeweiss, M. A.; Shanzer, A.; Vaskevich, A.; Rubinstein, I. *J. Am. Chem. Soc.* **2001**, *123*, 3177−3178.
(58) Bain, C. D.; Whitesides, G. M. *J. Am. Chem. Soc.* **1989**, *111*, 321−335.
(59) Chen, S. H.; Frank, C. W. *Langmuir* **1989**, *5*, 978−987.
(60) Wasserman, S. R.; Tao, Y. T.; Whitesides, G. M. *Langmuir* **1989**, *5*, 1074−1087.
(61) Tillman, N.; Ulman, A.; Schildkraut, J. S.; Penner, T. L. *J. Am. Chem. Soc.* **1988**, *110*, 6136−6144.
(62) Wenzel, R. N. *Ind. Eng. Chem.* **1936**, *28*, 988−994.

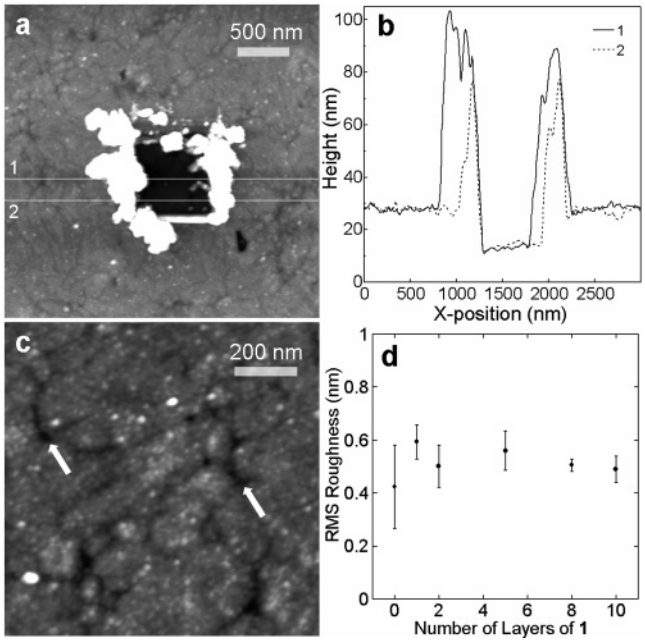


***Figure 5.*** (a) Dynamic mode AFM image of a window made by the AFM tip in a 10-layer multilayer of **1** on a SAM of **2** on Au. (b) Line sections through the window in (a), showing a film thickness of ~14 nm. (c) Higher resolution AFM image of an intact 10-layer film; the arrows indicate grain boundaries of the Au film (*z*-scale = 8 nm). (d) RMS roughness values for multilayers of **1**, calculated from AFM images (calculations performed on 200 × 200 nm$^2$ areas of single Au domains).

coordination multilayer of **1** on semitransparent, Au-coated quartz substrates by transmission UV−vis spectroscopy.[49] Figure 6a shows differential extinction spectra (after subtracting the spectrum of the bare Au substrate) during construction of eight layers of **1**. The presence of the multilayer on the metallic substrate results in a decreased overall reflection, seen as a decreased extinction in the visible−near UV range.[63] In the far UV region, this effect is outweighed by absorption of the ligand **1**, as evidenced by the stepwise increase in the film extinction with additional layers of **1**. Figure 6b presents plots of the differential extinction at two wavelengths, 208 nm (the absorption maximum of **1**) and 633 nm (nonabsorbing film), showing regular increases and decreases of the extinction, respectively, corresponding to regular buildup of the multilayer.

Ellipsometric measurements during construction of the multilayers showed a typical stepwise decrease in Δ accompanying addition of molecular layers of **1**.[27,29,64] Multilayer growth, expressed as increase in film thickness, was evaluated by four independent techniques, i.e., ellipsometry, transmission UV−vis spectroscopy, AFM profilometry,[29,65] and XPS measurements[66] (Figure 6c). The ellipsometric and spectroscopic measurements were both analyzed at a wavelength of 632.8 nm, using a multilayer refractive index of $n_f = 1.50$, $k_f = 0$, established in numerous previous studies.[27,64,67] For analysis of the spectroscopic data, the thickness of the bare Au substrate

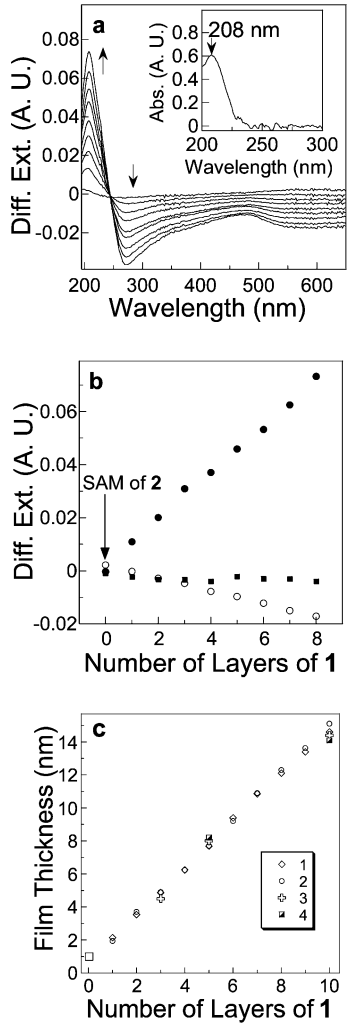


***Figure 6.*** (a) Differential extinction spectra (measured in air) during the construction of eight layers of **1** on a SAM of **2** on transparent, continuous 15-nm-thick Au film on quartz. The gray spectrum corresponds to the SAM of **2**. Inset: Absorption spectrum of 20 $\mu$M **1** in water ($\epsilon = 2.9 \times 10^4$ M$^{-1}$ cm$^{-1}$). (b) Differential extinctions at 208 nm (full circles) and at 633 nm (open circles), showing increasing extinction at 208 nm (absorbance of **1**) and decreasing extinction at 633 nm (change in reflection). Full squares correspond to a blank experiment at 633 nm, in which the regular adsorption steps on a SAM of **2** were replaced by immersion in the pure solvents (no **1** or Zr(acac)$_4$). (c) Film thickness values of coordination multilayers of **1** on a SAM of **2** on Au, obtained by (1) ellipsometry, (2) transmission spectroscopy, (3) AFM profilometry (±1 nm), and (4) XPS (using $\lambda = 3.3$ nm). Optical calculations were performed at $\lambda = 632.8$ nm, using a film refractive index $n_f = 1.50$, $k_f = 0$. The first point (square) is the ellipsometric thickness of a SAM of **2**.

was initially adjusted by fitting the experimental Au spectrum to a calculated glass/Au model, showing a good fit of the spectrum (see the Supporting Information).[68] A 3-layer model consisting of glass ($n$, $k$ = 1.52, 0), Au[69] ($n$, $k$ = 0.12, 3.29), and the film ($n$, $k$ = 1.50, 0) was then applied in order to calculate the multilayer film thickness.[70]

As seen in Figure 6c, the film thickness values obtained by the four different methods are practically identical, showing highly regular film growth. Results from AFM and XPS are

(63) Heavens, O. S. *Optical Properties of Thin Solid Films*; Dover Publications: New York, 1991.
(64) Lee, H.; Kepley, L. J.; Hong, H. G.; Akhter, S.; Mallouk, T. E. *J. Phys. Chem.* **1988**, *92*, 2597−2601.
(65) Wanunu, M.; Popovitz-Biro, R.; Cohen, H.; Vaskevich, A.; Rubinstein, I. *J. Am. Chem. Soc.* **2005**, *127*, 9207−9215.
(66) The overlayer thickness was calculated from the ratio of the total overlayer atomic signals to the Au substrate signal, using standard electron attenuation considerations.
(67) Bakiamoh, S. B.; Blanchard, G. J. *Langmuir* **1999**, *15*, 6379−6385.
(68) The experimental transmission spectrum of the bare Au was found to correspond to 21 nm Au, deviating from the nominal evaporation thickness (15 nm), as previously discussed in ref 49.
(69) *Handbook of Optical Materials*; Weber, M. J., Ed.; CRC Press: Boca Raton, FL, 2003.
(70) Differential transmission data were simulated by modeling the layers using Tfcalc software.

identical within experimental error, giving an average multilayer thickness increment of 1.3 nm ± 5% per layer. The results obtained by the two optical methods coincide within the experimental errors of the XPS and AFM data, confirming the appropriateness of the $n_f$ value chosen for the multilayer film.[71] The sample-to-sample variability in the slope of thickness versus number of layers is negligible, indicating excellent reproducibility. The observed 1.3 nm thickness increment per layer coincides with the expected height of a perpendicularly oriented molecular layer of **1** (see Figure 2b).

The increase of the extinction at 208 nm accompanying multilayer construction was exploited for estimating the surface density ($\gamma$) of **1** in each layer, using the relationship: $\gamma = 6.02 \times 10^6\, Ar/\epsilon$, where $\gamma$ is in molecules/nm$^2$, $r$ is the roughness factor of the substrate,[72] $\epsilon$ is the molar extinction coefficient of **1** (we used the value of $\epsilon$ measured in water), and A is the differential extinction per layer. This calculation gave a surface density of 1.3 molecules/nm$^2$, or 0.79 nm$^2$ per molecule of **1** in each layer, taking into account the roughness factor of the Au substrate ($r = 1.39$).[49] Since the real part of the refractive index of **1** in the UV region (corresponding to changes in film reflectivity) is not known, a true quantitative determination of the density of **1** in each layer is not possible, and the surface density calculated above is a lower limit. A more accurate determination of the multilayer absorbance requires simultaneous measurement of the transmission and reflection. Nevertheless, considering the measured thickness increment of 1.3 nm per layer (Figure 6c) that matches the perpendicular height of **1**, the absorbance results are consistent with formation of compact, vertically oriented layers of **1**.

Figure 1b depicts binding of molecule **1** to the underlying layer through one bis-hydroxamate arm, leaving the other two arms available for further coordination. However, attachment via two bis-hydroxamate arms bound to the underlying layer leaving one free arm is also possible. The latter mode imparts lateral cross-linking of the underlying layer, while the former mode (as in Figure 1b) provides the possibility of lateral cross-linking in the new layer, as well as lateral expansion over voids. Despite the different possible binding modes, branching and cross-linking, the end result is a highly regular multilayer growth with a constant, molecule-length thickness increment per layer.

**Evaluation of Cross-Linking in the Layers.** The suggested model of multilayer growth using branching molecules implies that the metal ions participate in attachment of the next layer, while also enabling lateral cross-linking between neighboring molecules. This proposed scheme suggests a unique structure, analogous to that of cross-linked, organometallic polymer films.[73] Various properties of the system, such as robustness, insulation, or defect management, are directly related to the extent of cross-linking in the layers, analogous to covalent cross-linking in organic polymers.

To substantiate the existence of lateral cross-linking in the multilayers, transmetalation experiments were carried out. Coordination binding of $Hf^{4+}$ is similar to that of $Zr^{4+}$,[28] enabling the use of $Hf^{4+}$ for transmetalation in the film, i.e., for probing the stability of metal ions in the film with respect to exchange with a different metal ion.

***Table 2.*** XPS Atomic Concentration Percent at Normal Takeoff Angles for Transmetalation Experiments

| adsorption sequence | C | O | N | Zr | Hf | S | Au |
|---|---|---|---|---|---|---|---|
| Experiment A | | | | | | | |
| **2**/$Zr^{4+}$ | 34.6 | 16.3 | 2.6 | 1.2 | | 2.0 | 43.0 |
| **2**/$Hf^{4+}$ | 35.0 | 15.5 | 2.4 | | 1.1 | 2.0 | 43.6 |
| **2**/$Zr^{4+}$/$Hf^{4+}$ | 37.0 | 16.6 | 2.4 | 0.3 | 1.3 | 2.5 | 40.3 |
| Experiment B | | | | | | | |
| **2**/$Zr^{4+}$/**3**/$Zr^{4+}$ | 33.3 | 17.3 | 3.5 | 1.8 | | 2.3 | 41.8 |
| **2**/$Zr^{4+}$/**3**/$Zr^{4+}$/$Hf^{4+}$ | 33.2 | 19.6 | 3.8 | 1.6 | 0.4 | 2.3 | 39.1 |
| Experiment C | | | | | | | |
| **2**/($Zr^{4+}$/**3**)$_2$/$Zr^{4+}$ | 33.8 | 21.3 | 4.6 | 2.2 | | 1.4 | 36.7 |
| **2**/($Zr^{4+}$/**3**)$_2$/$Zr^{4+}$/$Hf^{4+}$ | 34.1 | 21.8 | 4.7 | 2.1 | 0.3 | 1.3 | 35.7 |
| Experiment D | | | | | | | |
| **2**/$Zr^{4+}$/**1**/$Zr^{4+}$ | 36.2 | 15.5 | 4.1 | 1.6 | | 2.0 | 40.5 |
| **2**/$Zr^{4+}$/**1**/$Zr^{4+}$/$Hf^{4+}$ | 37.5 | 17.8 | 3.4 | 1.3 | 0.8 | 2.1 | 37.0 |
| Experiment E | | | | | | | |
| **2**/($Zr^{4+}$/**1**)$_2$/$Zr^{4+}$ | 43.1 | 24.0 | 5.9 | 2.7 | | 1.3 | 22.9 |
| **2**/($Zr^{4+}$/**1**)$_2$/$Zr^{4+}$/$Hf^{4+}$ | 43.2 | 25.8 | 5.8 | 2.6 | 0.5 | 1.4 | 20.6 |

Table 2 shows XPS atomic concentrations for transmetalation experiments in the early stages of construction of multilayers of the linear molecule **3** and branched molecule **1**. Experiment A corresponds to SAMs of the bis-hydroxamate anchor **2**. The compositions of SAMs of **2** coordinated with either $Zr^{4+}$ or $Hf^{4+}$ are consistent with the formation of a 1:1 ligand/ion complex (theoretical N/$M^{4+}$ ratio, 2:1; actual, 2.2:1), as previously demonstrated for a similar bis-hydroxamate monolayer.[29] Treatment of a $Zr^{4+}$-coordinated SAM of **2** with $Hf^{4+}$ shows that ca. 26% of the $Zr^{4+}$ ions remain in the layer, i.e., most of the binding sites in the SAM were exchanged with $Hf^{4+}$. Note that the total amount of metal ions in the SAM increased after the exchange beyond the number of available binding sites, i.e., N/(Hf + Zr) < 2, suggesting some nonspecific accumulation of $Hf^{4+}$.

Experiment B corresponds to transmetalation experiments carried out on one $Zr^{4+}$-terminated layer of the linear molecule **3**. After treatment with $Hf^{4+}$, an 18% decrease in the Zr/N ratio was observed. If the layer of **3** is not cross-linked, the $Zr^{4+}$ ions at the top of the layer would represent ~50% of the total $Zr^{4+}$ ions in the film, hence an 18% decrease in the total Zr/N ratio would represents a 36% transmetalation of the topmost layer with $Hf^{4+}$, much lower than the 74% exchange observed for a SAM of **2**. This result suggests a certain degree of cross-linking in the layer of **3**, as explained below. Experiment C, which corresponds to transmetalation on two layers of **3** terminated with $Zr^{4+}$, shows only a 7% decrease in the Zr/N ratio following treatment with $Hf^{4+}$. This result, indicating little transmetalation, suggests more extensive cross-linking in the second layer of **3.** Considering the structure of molecule **3**, which consists of four hydroxamate-terminated arms, cross-linking may involve tridentate binding of $Zr^{4+}$ ions using an additional hydroxamate arm from an adjacent molecule in the layer, thereby stabilizing the ion binding toward exchange. Cross-linking involving tetradentate binding is energetically unfavorable in this case.

Experiments D and E correspond to similar transmetalation experiments carried out on films comprising one or two $Zr^{4+}$-

(71) Thickness variations in the ellipsometric thickness on the order of ±0.3 nm were observed in the first layer of **1**, which may be attributed to variability in the density and/or orientation of **1** in the first layer.
(72) The roughness factor is defined as the ratio of real to geometric surface area.
(73) Archer, R. D. *Inorganic and Organometallic Polymers*; Wiley-VCH: New York, 2001.

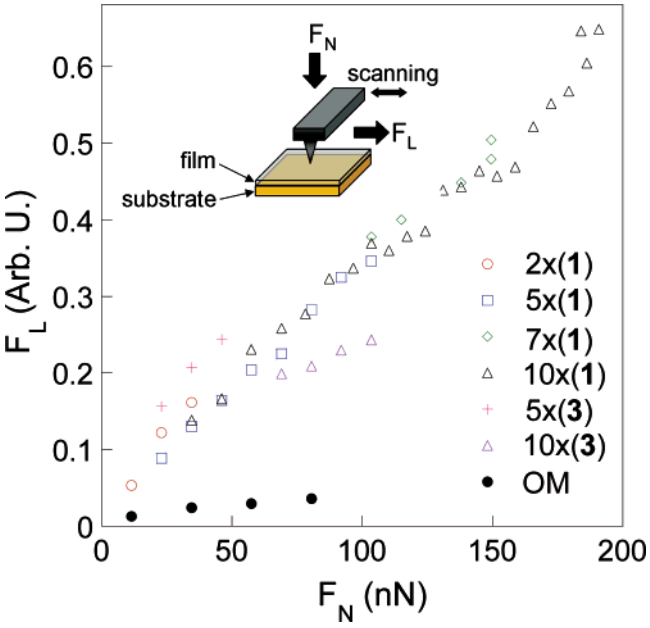


***Figure 7.*** AFM lateral ($F_L$) vs normal ($F_N$) force curves for different samples obtained in the wearless regime (before the breakpoint) for $Zr^{4+}$-coordinated multilayer films assembled on SAMs of **2** on Au. Similar measurements on an octadecylmercaptan (OM) SAM on Au are included as a reference. The legend gives the number of layers of **1** or **3** assembled on the SAM of **2**. Inset: Schematic presentation of the forces recorded in the measurements.

terminated layers of the branched molecule **1**. The results show a ca. 2% decrease in the Zr/N ratio for one and two layers of **1**. These results suggest extensive cross-linking even for one layer of **1**. In the case of molecule **1**, consisting of three bishydroxamate groups, cross-linking in the layer involves formation of a stable tetradentate $Zr^{4+}$ complex between two adjacent molecules.

The transmetalation results may be rationalized by considering the nature of the metal−organic bond. Binding of $Zr^{4+}$ to the SAM of **2** results in bidentate ligation to the metal ion through one bis-hydroxamate group (plus two weakly bound acac molecules), evidently enabling facile exchange with $Hf^{4+}$ ions. Binding of either **1** or **3** to the SAM of **2** occurs via tetradentate $Zr^{4+}$ ligation to two bis-hydroxamate groups, forming a more stable complex, not amenable kinetically to transmetalation. The fact that in experiments B−E (Table 2) most of the $Zr^{4+}$ ions were not exchanged implies, therefore, that hydroxamate groups not used for binding to the underlying layer are largely cross-linked, forming more stable multidentate bonds to $Zr^{4+}$, most likely tetradentate and tridentate in the case of molecules **1** and **3**, respectively. An additional test experiment (not shown) in which the opposite ion replacement was investigated, i.e., binding of $Hf^{4+}$ onto two $Zr^{4+}$-bound layers of **1**, followed by exposure to $Zr^{4+}$, resulted in similar, inefficient exchange. The transmetalation experiments therefore indicate that the formed layers are largely cross-linked. Assembly of the next layer of **1** or **3** requires opening of a fraction of the cross-links, i.e., breaking of multidentate coordination bonds. This applies primarily to layers of **3** and less so to layers of **1**, as the branching in the latter furnishes an excess of bishydroxamate groups in the layers.

**Mechanical Properties.** As noted above, the structure of multilayers comprising the branched molecule **1** and the linear molecule **3** appears to be different in two respects: the lateral

***Table 3.*** Normal and Lateral Breakpoint Forces for Coordination Multilayer Films Composed of Molecule **1** or **3** (Number of Layers Does Not Include the SAM of the Anchor **2**)

| | breakpoint force | | | |
|---|---|---|---|---|
| | **1** | | **3** | |
| no. of layers | normal (nN) | lateral (A. U.) | normal (nN) | lateral (A. U.) |
| 2 | 23 ± 1 | 0.16 ± 0.01 | | |
| 5 | 113 ± 2 | 0.35 ± 0.02 | 40 ± 1 | 0.24 ± 0.02 |
| 7 | 169 ± 4 | 0.48 ± 0.04 | | |
| 10 | 223 ± 5 | 0.88 ± 0.07 | 135 ± 3 | 0.39 ± 0.05 |

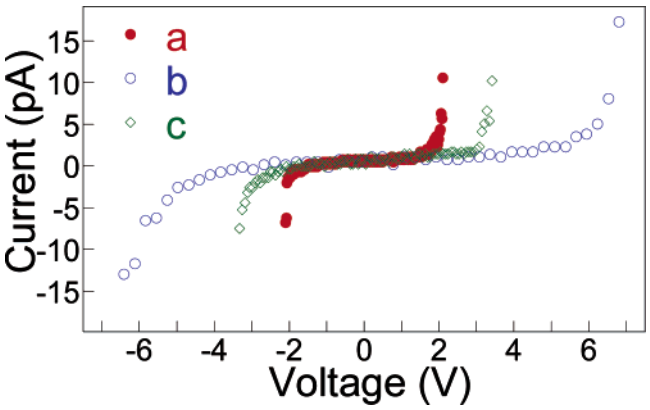


***Figure 8.*** Conductive AFM $I-V$ curves recorded under ambient conditions for a 3-layer (a) and 5-layer (b) multilayer of $Zr^{4+}$/**1** and a 5-layer multilayer of $Zr^{4+}$/**3** (c) on a SAM of **2** on Au.

cross-linking is tetradentate for layers of **1** and largely tridentate for layers of **3**; and the extent of cross-linking is higher in multilayers of **1** due to the excess hydroxamate groups provided by the branching. This difference in structure and stability is expected to affect the mechanical properties of the systems in terms of film stiffness. Hence, the mechanical properties of branched multilayer films composed of molecule **1** were investigated using AFM and compared with analogous multilayers composed of linear molecule **3**, the latter previously studied by our group.[27,29] The lateral force (friction) was monitored as a function of the applied normal force while scanning the film with a $SiO_2$-terminated tip (Figure 7, inset). Figure 7 shows friction ($F_L$) versus normal force ($F_N$) for the different multilayer films, recorded using forces below the film breakpoint. All the curves show a linear dependence of the friction on the normal force, with no specific distinction between multilayers of **1** and **3**.

Whereas linear friction behavior on a macroscopic scale has been ascribed to increasing contact area with force due to plastic[74] or elastic[75] deformations, continuum mechanical models predict a nonlinear behavior for a single asperity under elastic contact. For example, a $^2/_3$ power dependence was observed for epitaxial $C_{60}$ monolayers, which conforms to Herzian elasticity formulas for a spherical tip.[76] On the other hand, linear dependence was also observed on this scale.[52,77] Friction is a complex physicochemical phenomenon, with various casual factors including surface morphology, viscoelastic properties,

(74) Bowden, F. P.; Moore, A. J. W.; Tabor, D. *J. Appl. Phys.* **1943**, *14*, 80−91.
(75) Greenwood, J. A.; Williamson, J. *Proc. R. Soc. London* **1966**, *295*, 300−319.
(76) Schwarz, U. D.; Allers, W.; Gensterblum, G.; Wiesendanger, R. *Phys. Rev. B* **1995**, *52*, 14976−14984.
(77) Liu, Y. H.; Wu, T.; Evans, D. F. *Langmuir* **1994**, *10*, 2241−2245.

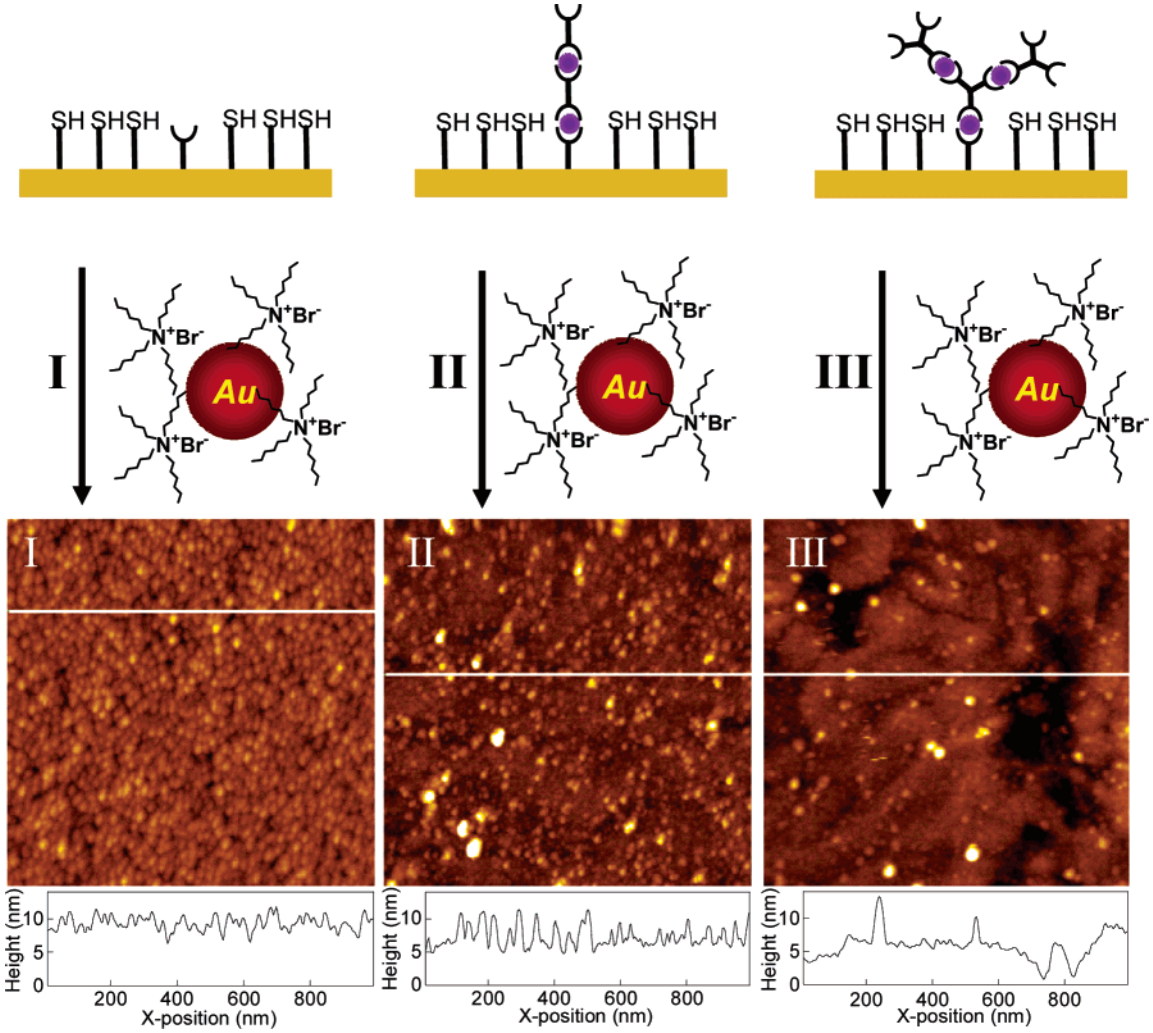


***Figure 9.*** Binding of TOAB-capped NPs to a mixed SAM of **2** and DDT on Au, prior to (I) and following binding of two $Zr^{4+}$-coordinated layers of either the linear ligand **3** (II) or the branching ligand **1** (III). Corresponding AFM images of I−III ($1 \times 1$ $\mu m^2$) are shown with line profiles.

surface free energy, lubrication by films, and chemical reactivity.[78] While similarity in the friction behavior (i.e., the $F_L/F_N$ slope in Figure 7) between multilayers of **1** and **3** (Figure 7) could therefore be fortuitous, it is strongly indicative of similar surface properties, such as surface energy[79] and rigidity,[80] of the two hydroxamate-terminated films. Since no significant frictional variations are observed in different surface regions during scanning (not shown), the recorded friction is assumed to reflect the homogeneous mechanical properties of the multilayer films.[81] For comparison, a force/friction curve for a monolayer of OM is also shown in Figure 7. The friction values of OM are approximately an order-of-magnitude lower. The apparently larger shear strength of the hydroxamate-terminated films could arise both from the higher surface energy and from the different structure-related mechanical behavior relative to the highly ordered, methyl-terminated OM surface. Adhesion measurements carried out with the AFM (not shown) indicated that only minor differences in surface energy exist between multilayers of **1** and **3**.

The breakpoint forces for the different multilayer films are given in Table 3. The robustness of the films increases with the number of layers in all cases. Here the data show distinct differences between linear (**3**) and branched (**1**) multilayers: for the 5- and 10-layer multilayers, $F_N$ at breakpoint is larger for the branched molecule by 180% and 65%, respectively. This seems to be a direct consequence of the lateral cross-linking, more prevalent and more stable in the branched multilayers than in the linear ones, as discussed above.

**Electrical Properties.** The electrical properties of branched coordination layers of $Zr^{4+}$/**1** were evaluated using conductive-tip AFM measurements. Figure 8 shows AFM $I-V$ curves for three and five coordinated layers of **1** on a SAM of **2** on Au. The curves show a typical resistance to electron transfer, exhibiting a symmetric breakdown voltage of ca. ±2 V for three layers of **1** and ca. ±6 V for five layers of **1**. The results were highly reproducible on the same spot (when the current was limited to <10 pA) and at different locations on the sample. The measured resistance for three layers of **1** is ca. $10^{12}$ Ω (derived from the slope of the $I-V$ curve in the low bias range, before breakdown), similar to that reported by us for three layers of **1** coordinated to a top layer of Au NPs.[65] This suggests that the resistance of direct tip-to-films contact is not significantly

(78) Bhushan, B. *Introduction To Tribology*; Wiley: New York, 2002.
(79) Also observed by wettability measurements, not shown here.
(80) Overney, R. M.; Meyer, E.; Frommer, J.; Brodbeck, D.; Luthi, R.; Howald, L.; Guntherodt, H. J.; Fujihira, M.; Takano, H.; Gotoh, Y. *Nature* **1992**, *359*, 133−135.
(81) Bhushan, B.; Kulkarni, A. V.; Koinkar, V. N.; Boehm, M.; Odoni, L.; Martelet, C.; Belin, M. *Langmuir* **1995**, *11*, 3189−3198.

different from that achieved via a layer of NPs, in contrast to results reported for alkanethiol SAMs.[82] For comparison, an $I-V$ curve for a 5-layer multilayer of $Zr^{4+}$/**3** is shown (Figure 8c). The $I-V$ curve is qualitatively similar to those of the multilayers of **1**, with a breakdown voltage of ca. ±3 V.

The electrical data show that the multilayers function as efficient dielectric films, with a breakdown voltage that can be tuned by the number of layers. The electric field at breakdown, calculated using the measured multilayer thicknesses (Figure 6), is 5 MV/cm to 8 MV/cm (for three and five layers of **1**, respectively) and 4.5 MV/cm (for five layers of **3**, using a thickness of ca. 6.5 nm[83]). These values are of the same order as breakdown values of ultrathin silicon oxide films,[84] as well as values reported for electrical breakdown of several organic monolayer systems.[85,86] Although the results suggest a higher breakdown field for multilayers of **1** compared to **3**, a definite conclusion requires additional experiments.

**Defect Self-Repair.** Branching and efficient lateral cross-linking promoted by the excess hydroxamate groups, as shown to proceed in multilayer construction using ligand **1**, point to the enticing possibility of lateral growth over defects and voids, which would act as a unique self-repair mechanism during multilayer formation. To investigate lateral growth over defects in LbL assembly of coordination multilayers of **1**, the experiment presented schematically in Figure 9 was carried out. A mixed SAM of the anchor **2** and 1,10-decanedithiol (DDT) was prepared on semitransparent Au substrates (see the Experimental Section). The DDT domains in the mixed SAM serve to simulate defects in the monolayer of **2**, providing sites which are inert to coordination and further growth of the multilayer. Exposed DDT domains can be detected by interaction with TOAB-stabilized Au NPs (5 nm average core diameter), which bind to the terminal thiol groups but not to molecules **2**.[87] Two blank experiments were carried out: (i) Immersion of a SAM of **2** in a solution of the Au NPs resulted in no binding of NPs to the hydroxamate-terminated surface, showing that the NPs bind selectively to DDT molecules in the mixed SAM. (ii) Immersion of a mixed SAM of **2** and DDT in a $Zr^{4+}$ solution prior to NP binding had no effect on the amount of bound NPs, showing no influence of bis-hydroxamate−$Zr^{4+}$ coordination on the thiol−NP reaction. Differential spectra for the blank experiments are shown in the Supporting Information.

AFM image I (Figure 9) shows a nearly full layer of Au NPs bound to the initial mixed SAM, indicating that the DDT "defects" are homogeneously distributed over the scanned surface. When two layers of either the linear (**3**) or branched (**1**) ligand were coordinatively assembled onto the mixed SAM, the amount of bound NPs was drastically reduced, as seen in images II and III, respectively, indicating partial blocking of DDT defect sites by the two coordinated layers. The images

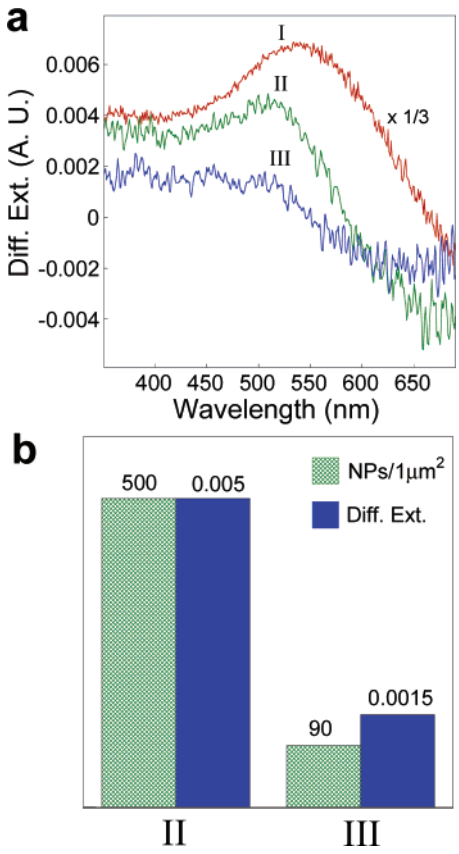


***Figure 10.*** (a) Differential extinction spectra of samples I−III (Figure 9). (b) Comparison of the NP density (from AFM) and the uncorrected differential extinction at $\lambda = 510$ nm, for samples II and III.

show a striking difference between II and III in the density of bound NPs: the surface treated with the linear molecule **3** (image II) shows considerably higher density of NPs than the surface treated with the branching molecules **1** (image III), demonstrating the superior defect repair process taking place in the branched layers. The line profiles through images I−III (shown under the images) emphasize the different NP densities. The height of the features, as seen in the line sections, is 5−7 nm, matching the size of the NPs.[65] Some large bright spots (ca. 10 nm high) are visible in images II and III, which are attributed to aggregated NPs.

Figure 10a presents differential extinction spectra of samples I−III (Figure 9), showing an extinction band characteristic of the localized surface plasmon absorption of Au NPs. The band intensity decreases from I to III, corresponding to the NP density in the AFM images. Spectrum I is red-shifted from 510 nm (spectra II, III) to 540 nm, attributed to the close-packing of the NPs seen in AFM image I. A summary of the differences between samples II and III is given in Figure 10b, showing NP density (obtained by counting NPs in the AFM images) and differential extinction (from the absorbance maxima). The two parameters are 5.5 and 3.4 times larger, respectively, in sample II.[88] It is therefore evident from both the microscopic and macroscopic measurements that branched molecule **1** blocks the DDT defect sites much more efficiently than linear molecule **3**, confirming the effective defect self-repair mechanism in the branched layer assembly.

(82) Cui, X. D.; Primak, A.; Zarate, X.; Tomfohr, J.; Sankey, O. F.; Moore, A. L.; Moore, T. A.; Gust, D.; Harris, G.; Lindsay, S. M. *Science* **2001**, *294*, 571−574.
(83) Wanunu, M.; Vaskevich, A.; Cohen, H.; Shanzer, A.; Rubinstein, I., **2005**, manuscript in preparation.
(84) Chen, I. C.; Holland, S.; Young, K. K.; Chang, C.; Hu, C. *Appl. Phys. Lett.* **1986**, *49*, 669−671.
(85) Wold, D. J.; Frisbie, D. *J. Am. Chem. Soc.* **2001**, *123*, 5549−5556.
(86) Holmlin, R. E.; Haag, R.; Chabinyc, M. L.; Ismagilov, R. F.; Cohen, A. E.; Terfort, A.; Rampi, M. A.; Whitesides, G. M. *J. Am. Chem. Soc.* **2001**, *123*, 5075−5085.
(87) The $C_{10}$ dithiol was chosen so that its extended length is slightly larger than the length of **2**, to ensure that binding of Au NPs is not sterically constrained in the mixed SAM.
(88) The AFM results are more reliable since determination of the true absorbance by the NPs requires correction for reflection losses.

## Conclusions

A viable approach to the construction of coordination-based multilayers displaying unique properties has been demonstrated. The $C_3$-symmetrical ligand **1**, possessing three bis-hydroxamate ligand arms, was synthesized and utilized in the LbL construction of branched coordination multilayers on semitransparent Au. Functionalization of the Au surface with a SAM of bis-hydroxamate anchor molecules, followed by alternate binding of layers of **1** and $Zr^{4+}$ ions, produced coordination multilayer films. The branched multilayers were characterized by a variety of techniques and their structural, mechanical, and electrical properties studied. Multilayer growth proceeds in a highly regular fashion, showing characteristic oscillating wettability and a constant thickness increment per added layer, corresponding to the size of one perpendicularly oriented molecule. Extensive intermolecular cross-linking was found in the layers, indicated by inefficient transmetalation of the coordinated layers with an equivalent metal ion. The excess hydroxamate groups introduced by the branching, effecting more pronounced cross-linking, is suggested to be responsible for the improved mechanical properties over analogous, linear multilayers. The electrical properties of the multilayers are typical of highly efficient, low-leakage dielectric insulators, exhibited by breakdown fields of 5−8 MV/cm.

The concept of branching in multilayers introduces a space-filling element which affords lateral expansion, bridging between spaced molecules, and continuous repair of voids and other defects during multilayer formation. The latter property was demonstrated via efficient masking of intentional thiol defects introduced into an anchor SAM, showing that two branched layers blocked Au NP binding to the defect surface thiols much more efficiently than two analogous linear layers.

Highly controlled LbL construction of ultrathin films coupled with cross-linking and effective lateral growth over defects is an intriguing concept which may be important for various purposes, such as electronic applications requiring nanometer-scale pinhole-free dielectric layers, as well as formation of continuous, homogeneous layers on nonplanar and corrugated surfaces. The special qualities of branched coordination multilayers demonstrated here may open the way to the development of improved and more applicable multilayer systems.

**Acknowledgment.** Support from the Israel Science Foundation, Grant No. 307/03, and the Israel Ministry of Science, Tashtiot Infrastructure Project No. 01-01-01470, is gratefully acknowledged. M.W. is recipient of a Levy Eshkol Doctoral Fellowship, Israel Ministry of Science. We thank Dr. Rachel Persky for the FAB/HRMS measurements.

**Supporting Information Available:** Synthetic procedures for the preparation of molecule **1** (including FAB/HRMS and $^1$H NMR); FTIR, ES/MS spectra of **1**; experimental and calculated extinction spectra of the transparent Au film on aminosilanized glass; differential extinction spectra for blank experiments. This material is available free of charge via the Internet at http://pubs.acs.org.

JA0556676